Catalysis of Stark-tuned Interactions between Ultracold Rydberg Atoms

Department of Physics
University of Virginia

Aye Lu Win
Department of Physics
Old Dominion University

March 1 2016

Outline

- Interactions between ultracold Rydberg atoms
- Stark-tuned Förster resonances
- Laser cooling and trapping with magneto-optical trap
- Experimental setup
- Time dependence of resonant energy transfer process and observation of a catalysis effect in the resonant energy transfer between ^{85}Rb Rydberg atoms

Rydberg Atoms

- Atoms in the highly excited states
- Large radius and large dipole-moment
- Strong long-range dipole-dipole interactions
- Long radiative lifetime
- Many-body physics and quantum information processing
- Studies of resonant energy transfer interactions

Rydberg atoms

Table: Properties of Rydberg atoms. Adapted from [2].

Property	n^* dependence
Binding energy	n^{*-2}
Energy between adjacent states	n^{*-3}
Ionizing field	n^{*-4}
Orbital radius	n^{*2}
Geometrical cross-section	n^{*4}
Dipole moment	n^{*2}
Polarizability	n^{*7}
Radiative lifetime	n^{*3}

Interaction between Rydberg atoms

Dipole-dipole interaction

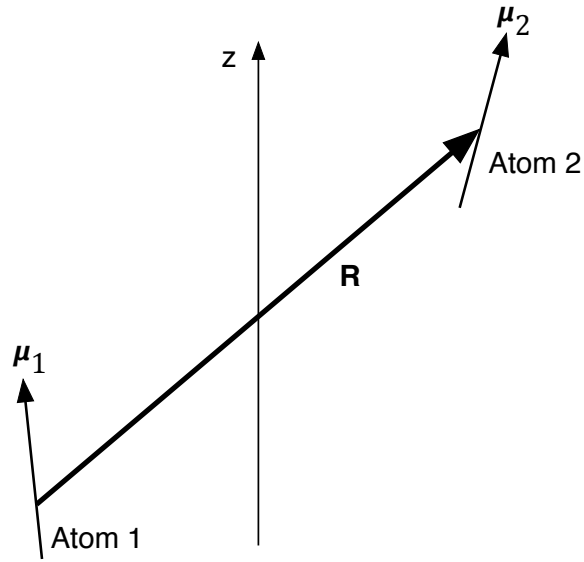

Figure: Schematic diagram of two interacting dipoles separated by a distance R.

$$V_{dd}(R) = \frac{\boldsymbol{\mu}_1 \cdot \boldsymbol{\mu}_2}{R^3} - \frac{3(\boldsymbol{\mu}_1 \cdot \mathbf{R})(\boldsymbol{\mu_2} \cdot \mathbf{R})}{R^5}$$

Interaction between Rydberg atoms

$$34p + 34p \rightarrow 34s + 35s$$

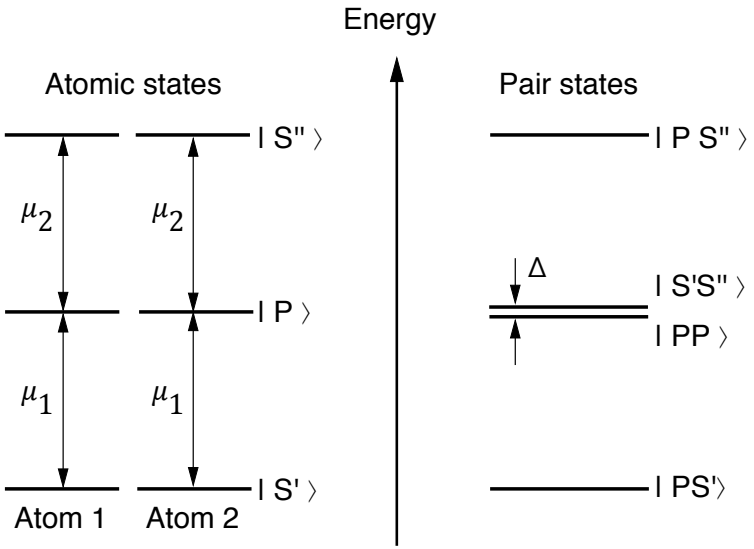

Figure: Transforming atomic state basic into pair state basic reveals two states that are almost degenerate with a small energy difference $\triangle$ called Förster defect.

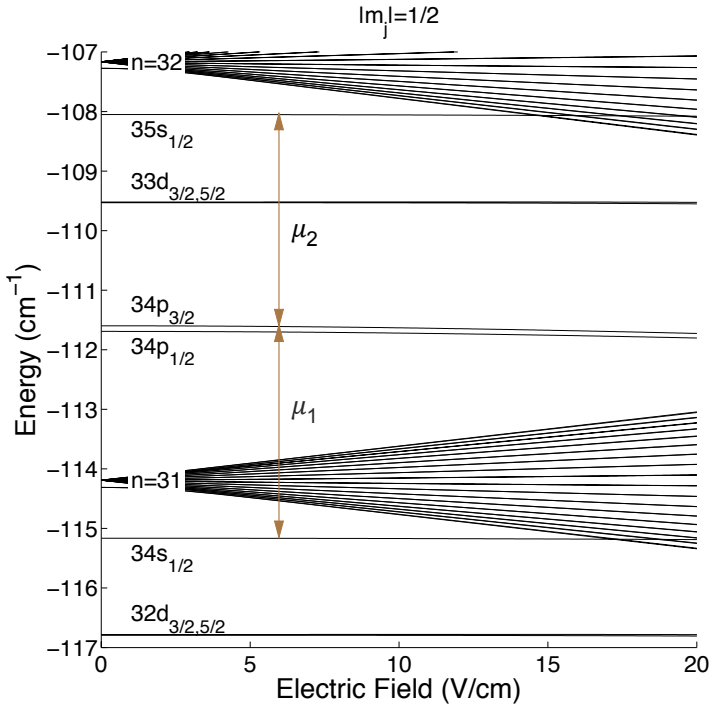

Figure: Stark structure of ^{85}Rb showing the dipole-coupled states of $34s_{1/2}$ and $34p_{3/2}$ with the dipole matrix element μ_1 and $34p_{3/2}$ and $35s_{1/2}$ with the dipole matrix element μ_2.

Interaction between Rydberg atoms

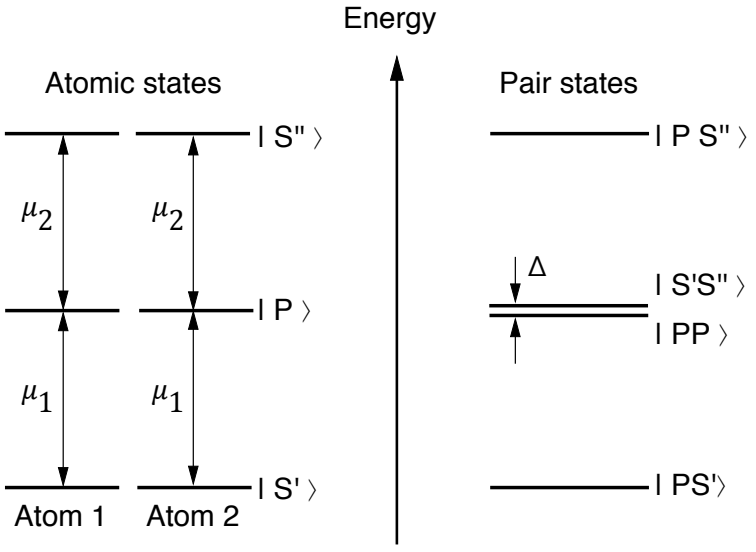

When $V_{dd}(R) \ll \triangle$, **van der Waals regime**

$$\begin{aligned}\triangle W_{vdW} &= -\frac{V_{dd}^2(R)}{\triangle} \\ &= -\frac{(\mu_1\mu_2)^2/\triangle}{R^6} \\ &= -\frac{C_6}{R^6}\end{aligned}$$

When $\triangle \ll V_{dd}(R)$

Resonant dipole-dipole interaction

$$\begin{aligned}\triangle W &= \pm V_{dd}(R) \\ &= \pm\frac{\mu_1\mu_2}{R^3} \\ &= \pm\frac{C_3}{R^3}\end{aligned}$$

$$H = \begin{pmatrix} 0 & V_{dd}(R) \\ V_{dd}(R) & \triangle \end{pmatrix}$$

with eigenvalues

$$\lambda_\pm = \frac{\triangle \pm \sqrt{\triangle^2 + 4V_{dd}^2(R)}}{2}$$

Stark-tuned Förster resonances

$$34p + 34p \rightarrow 34s + 35s$$

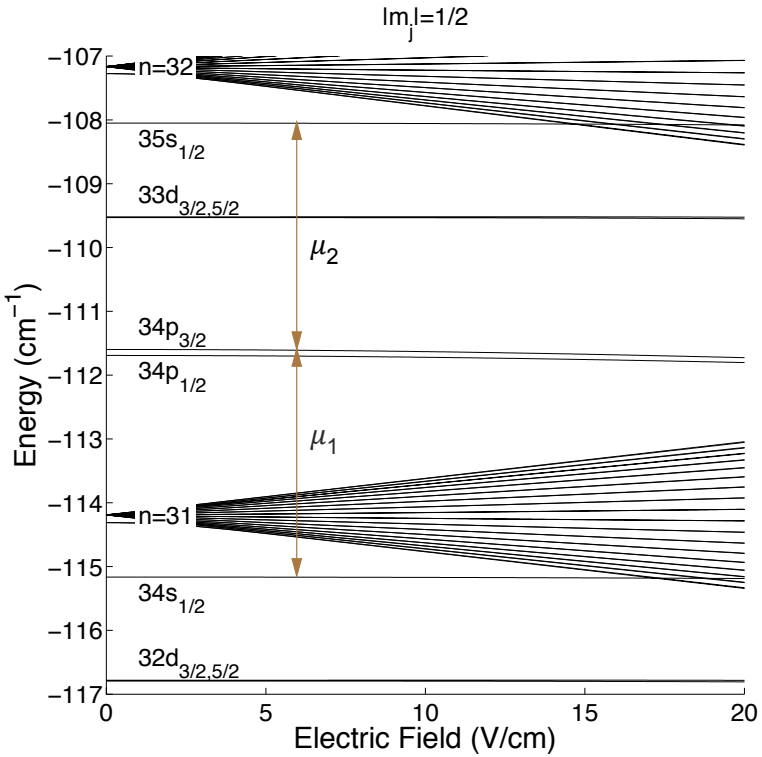

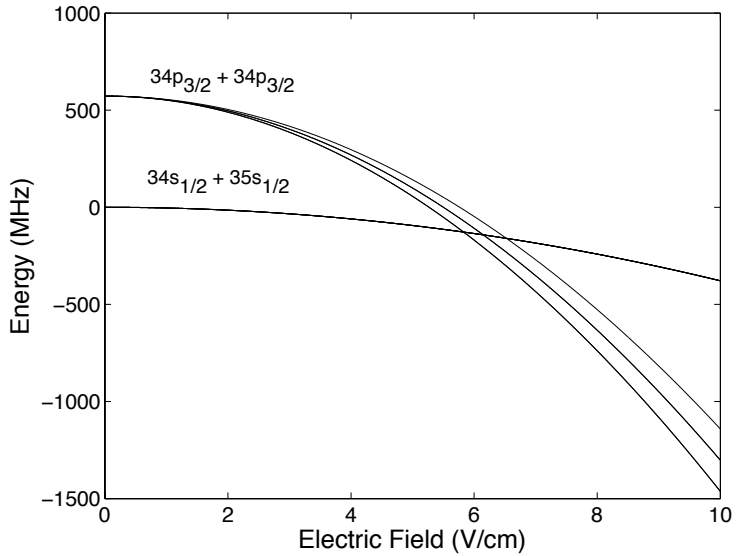

Figure: Stark structures of the pair states. Förster resonances are observed at the fields where the level crossings occur.

Laser cooling and trapping

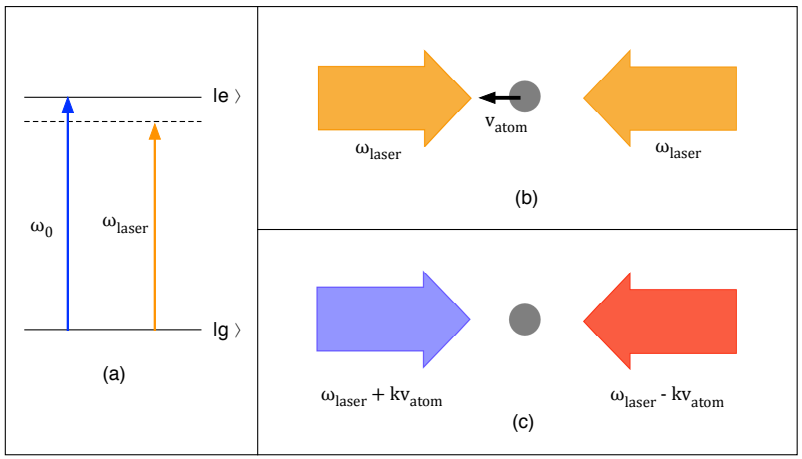

Figure: Doppler cooling scheme.

Magneto-optical trap

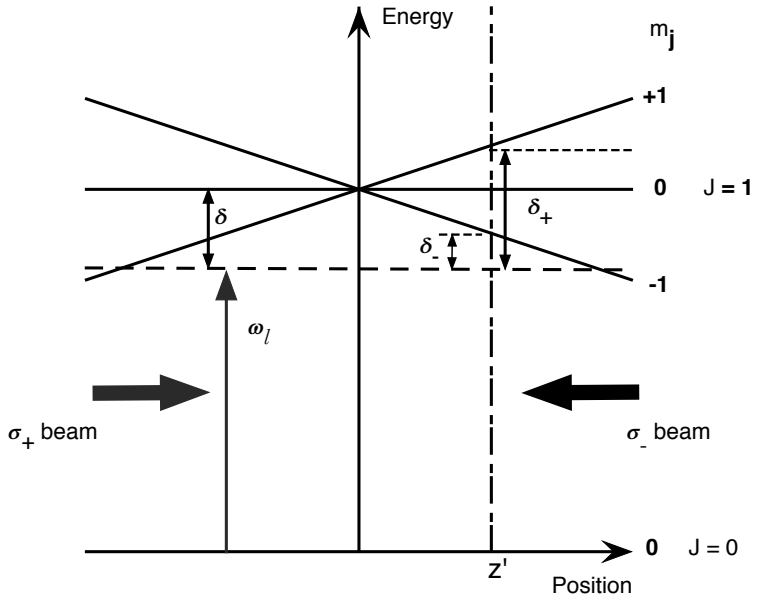

Figure: The principle of magneto-optical trapping [4].

Laser systems for magneto-optical trap

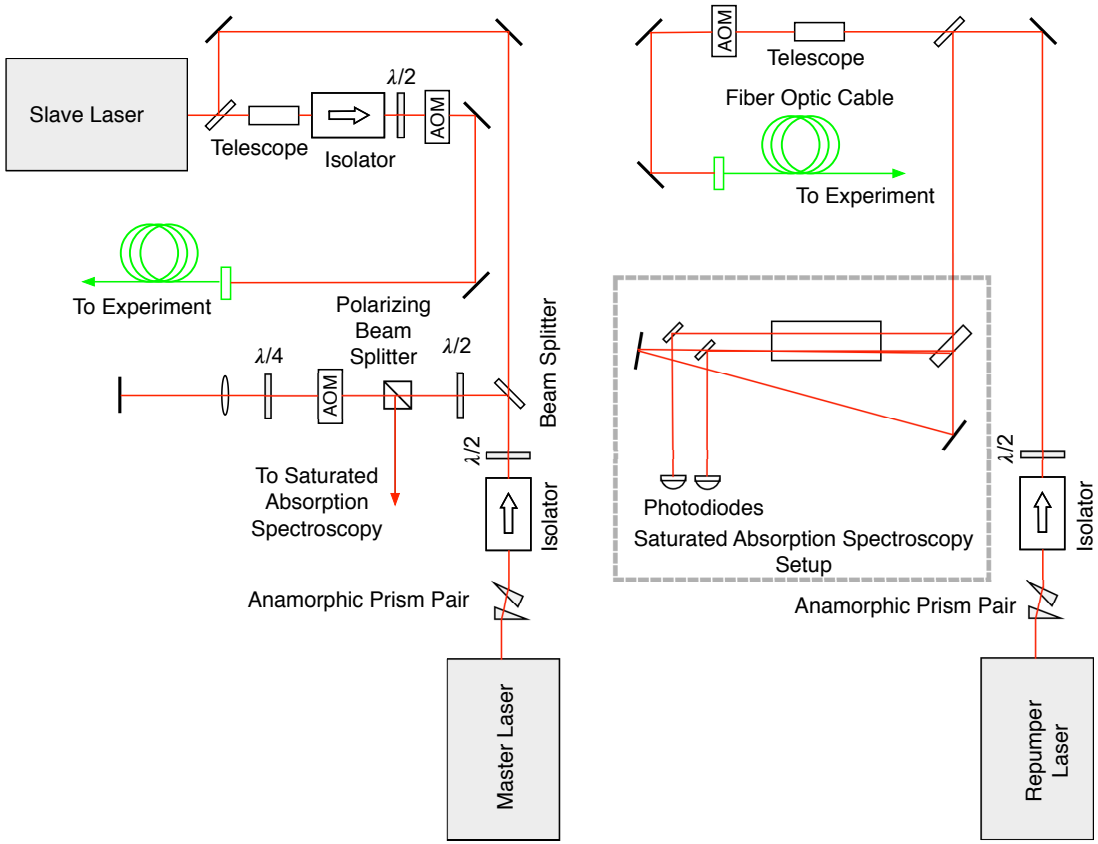

Figure: Schematic layout of the laser systems for magneto-optical trap.

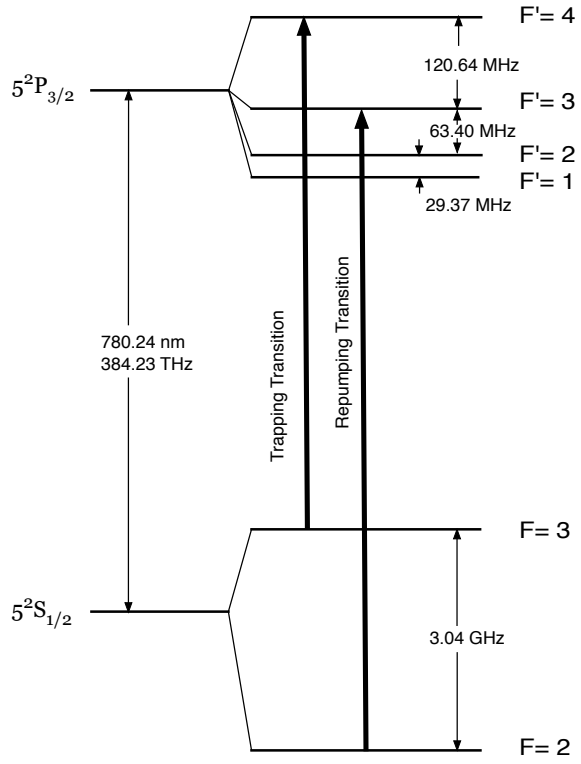

Figure: The energy levels of ^{85}Rb for magneto-optical trapping. Adapted from [7].

Laser systems for excitation to Rydberg states

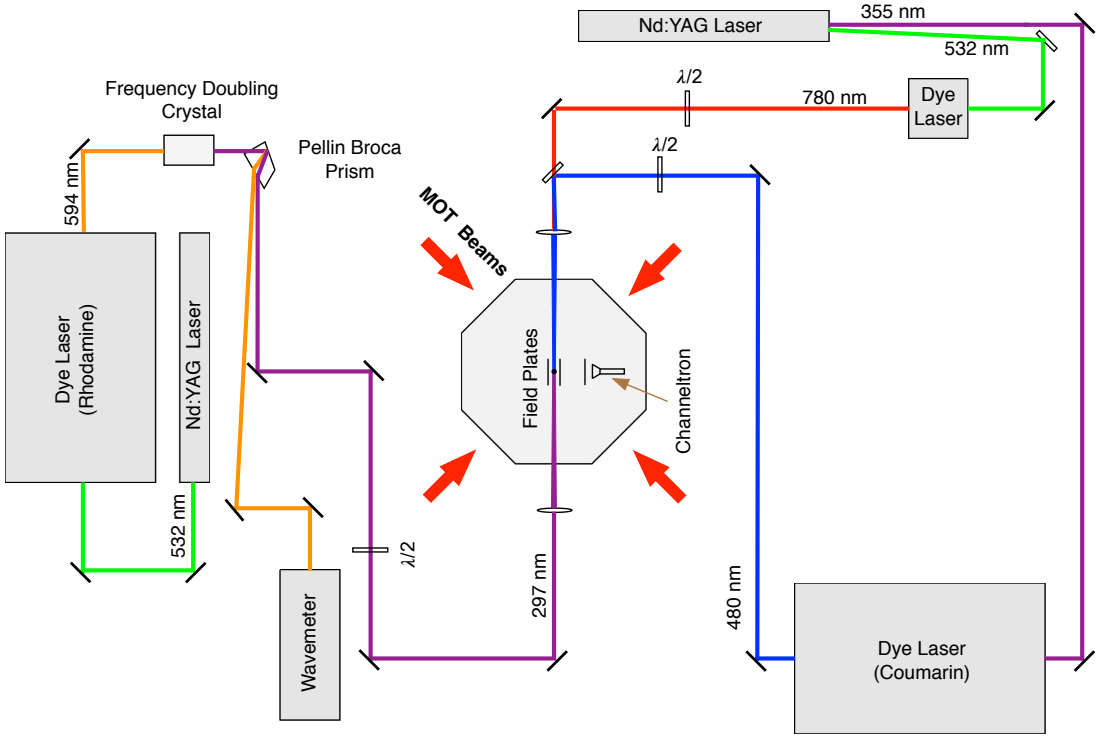

Figure: The schematic diagram of the optical setup of the laser systems for excitation of Rydberg states.

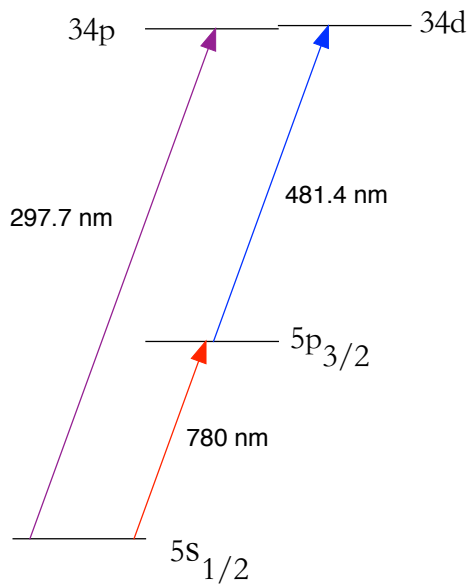

Figure: Rydberg excitation scheme.

Laser systems for excitation to Rydberg states

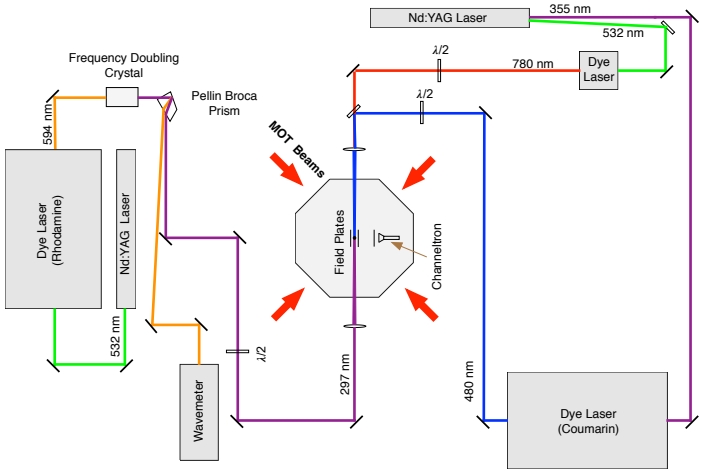

Figure: The schematic diagram of the optical setup of the laser systems for excitation of Rydberg states.

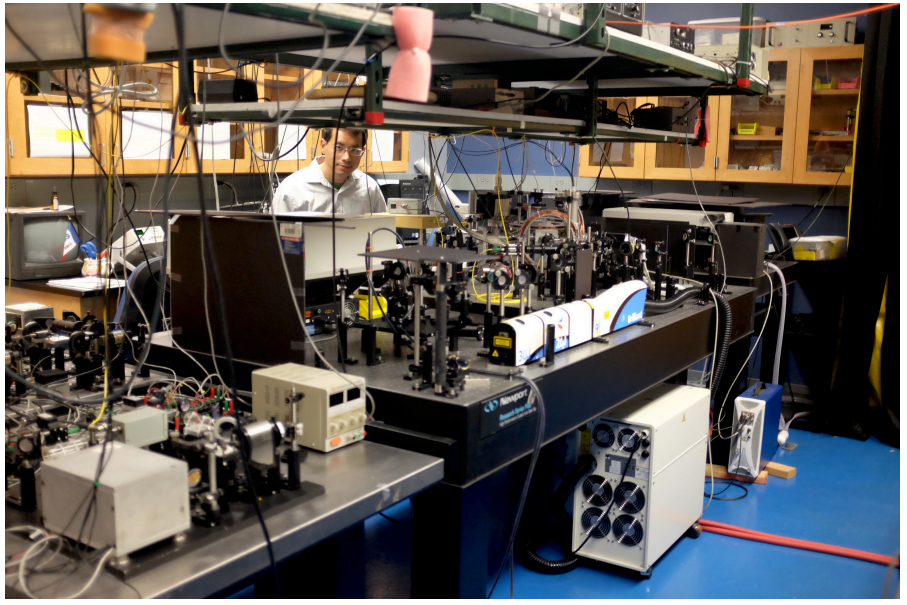

Tuning curve of the commercial dye laser

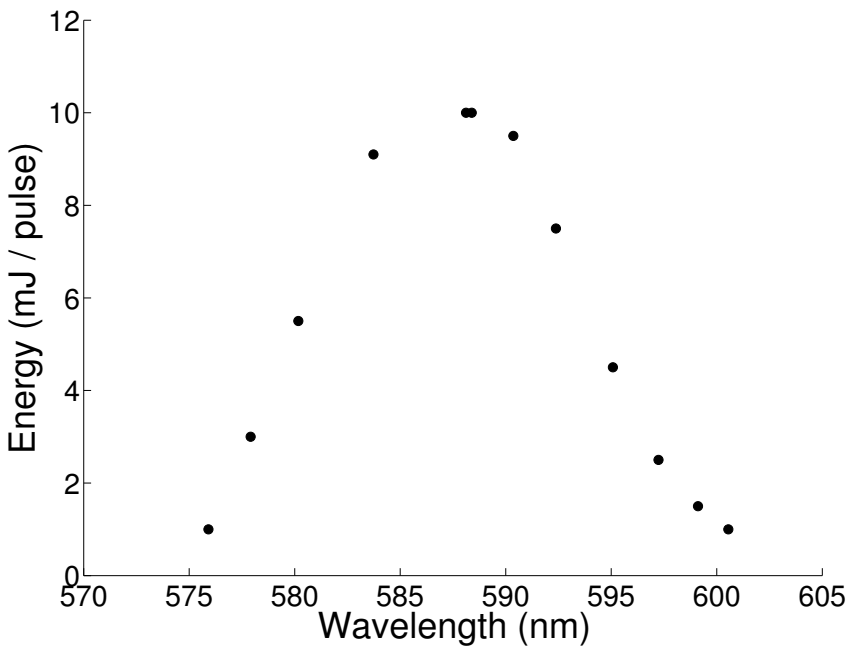

Figure: Tuning curve of Continuum ND6000 laser with Rhodamine 6G dye.

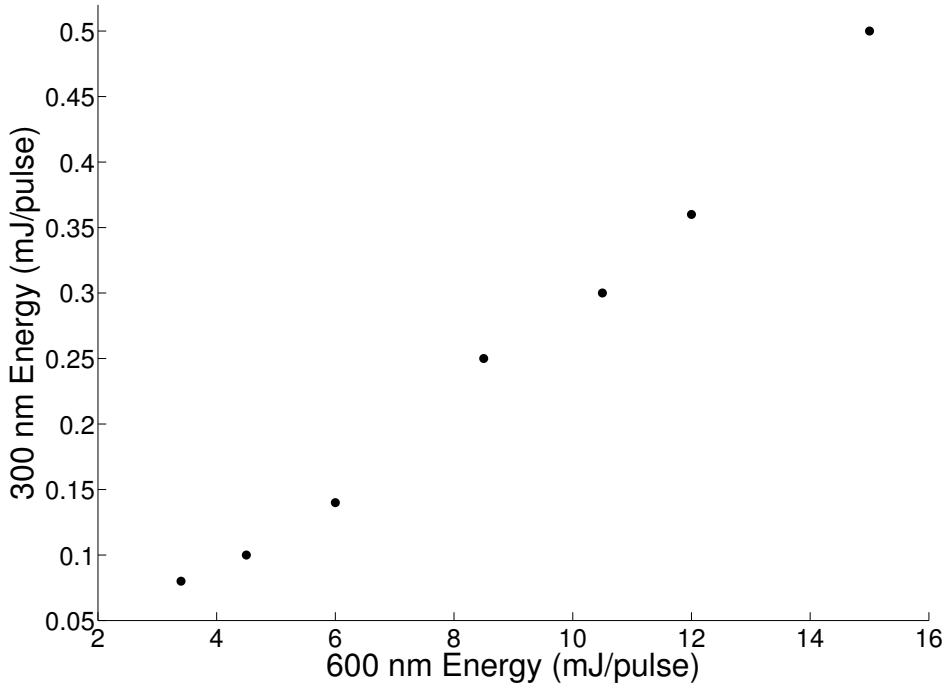

Figure: The output laser energy from the frequency doubling crystal vs. the input laser energy.

Tunable homebuilt dye laser

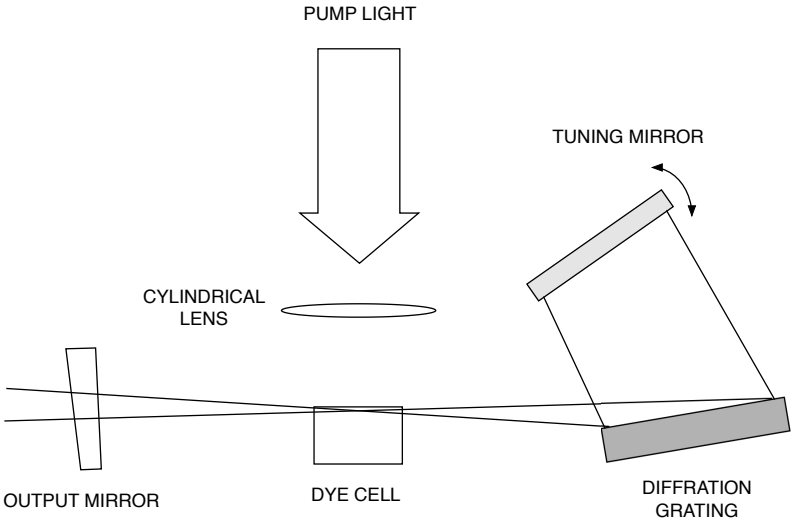

Figure: Schematic drawing of homebuilt dye laser in Littman configuration [3].

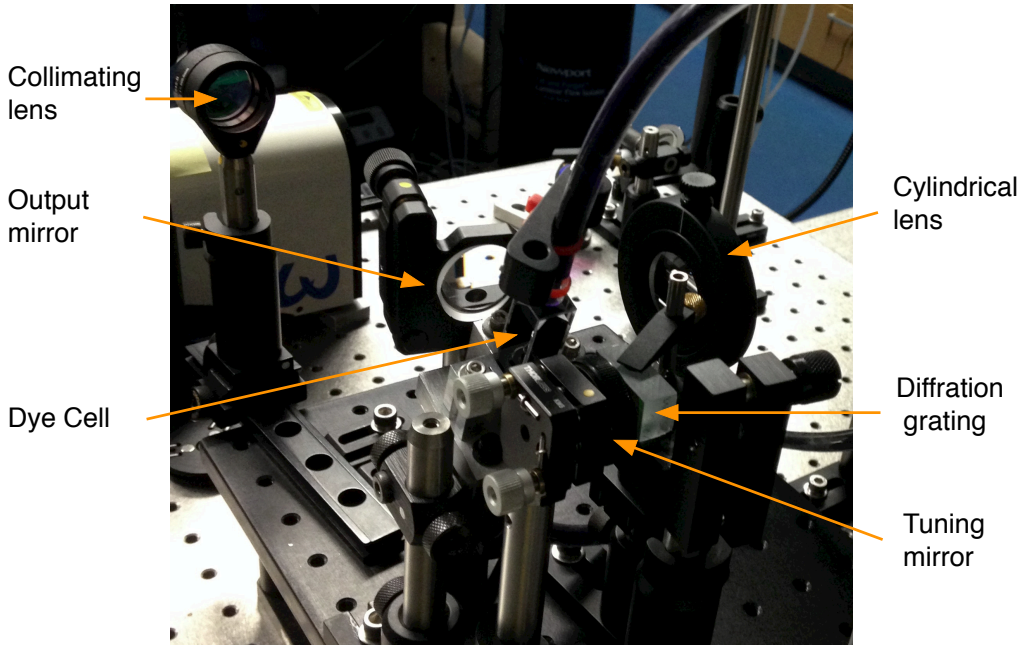

Figure: Tunable homebuilt dye laser.

Trap loss spectroscopy with fluorescence detection

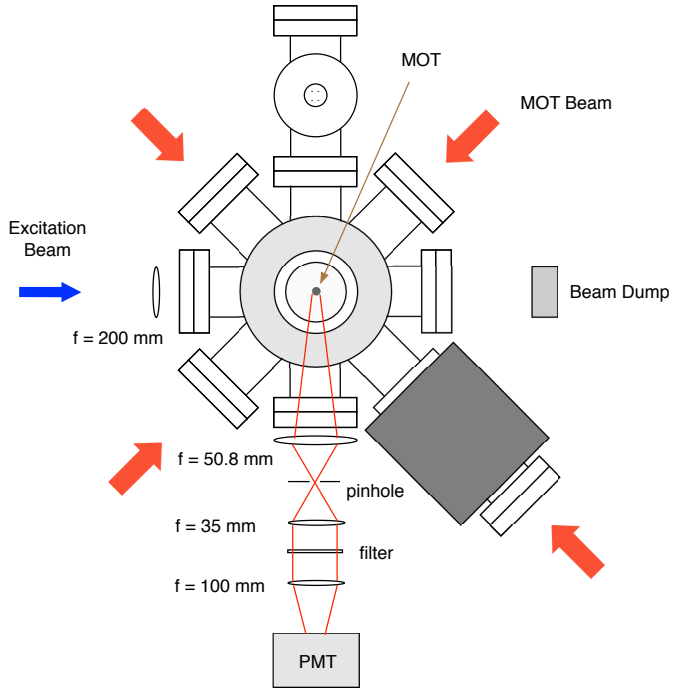

Figure: Schematic diagram of the optical setup for fluorescence detection.

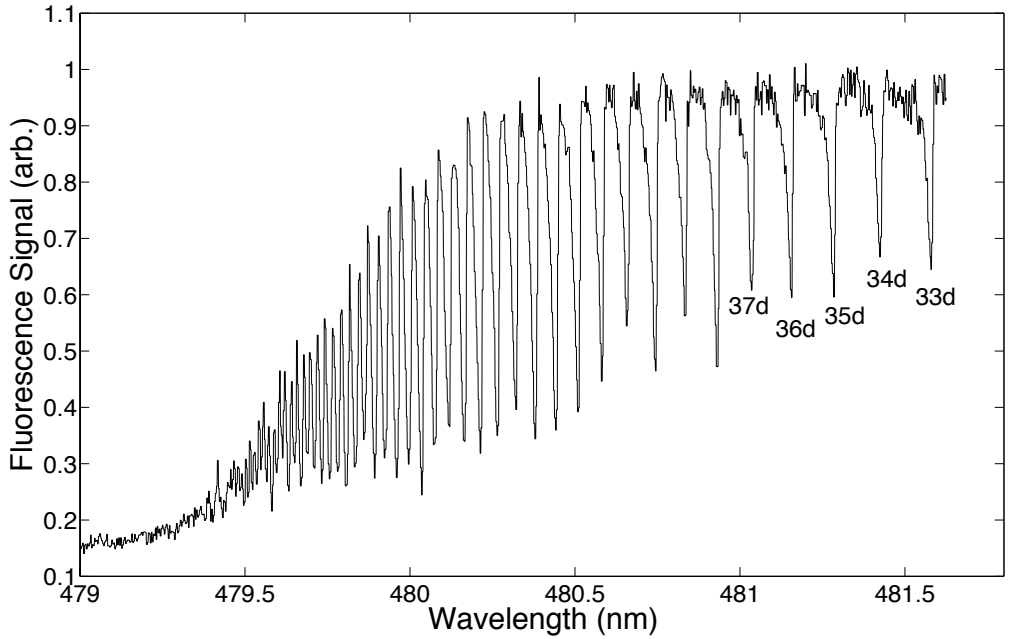

Figure: Trap loss spectroscopy.

Detection of Rydberg atoms with field ionization

- The potential for the valance electron of the Rydberg atoms in an external field, E, in the $\mathbf{z}$ direction

$$V = -\frac{1}{|z|} + Ez$$

- It has a saddle point at $z = -1/\sqrt{E}$ with the value of $V = -2\sqrt{E}$.
- Ionization occurs when V is greater than the binding energy.
- The threshold field for ionization,

$$E = \frac{1}{16n^{*4}}$$

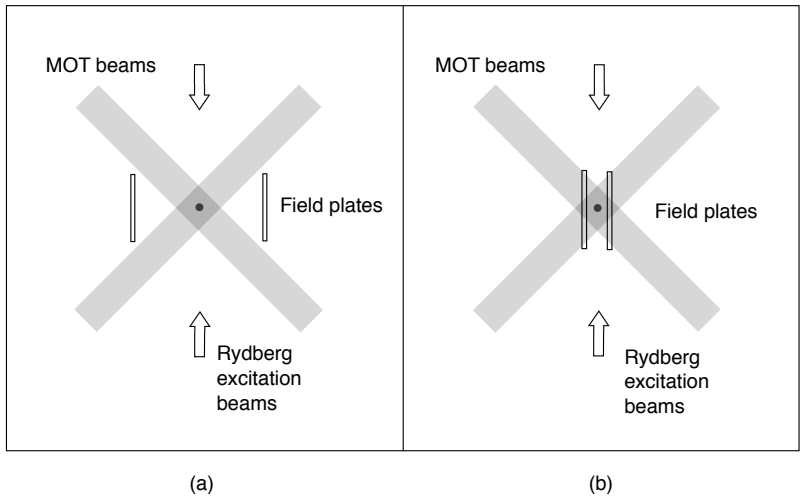

Figure: Schematic diagram for the top view of the two configurations of electric field plates for detection of Rydberg states by field ionization method.

Detection of Rydberg atoms with field ionization

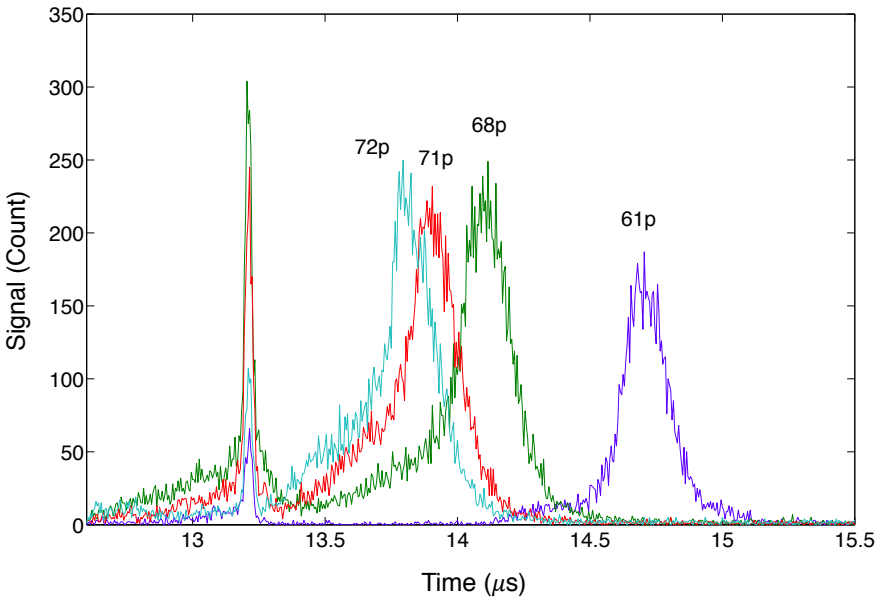

Figure: Time-resolved signals of Rydberg states detected by the field ionization method with plate separation of $\sim$ 4.6 cm.

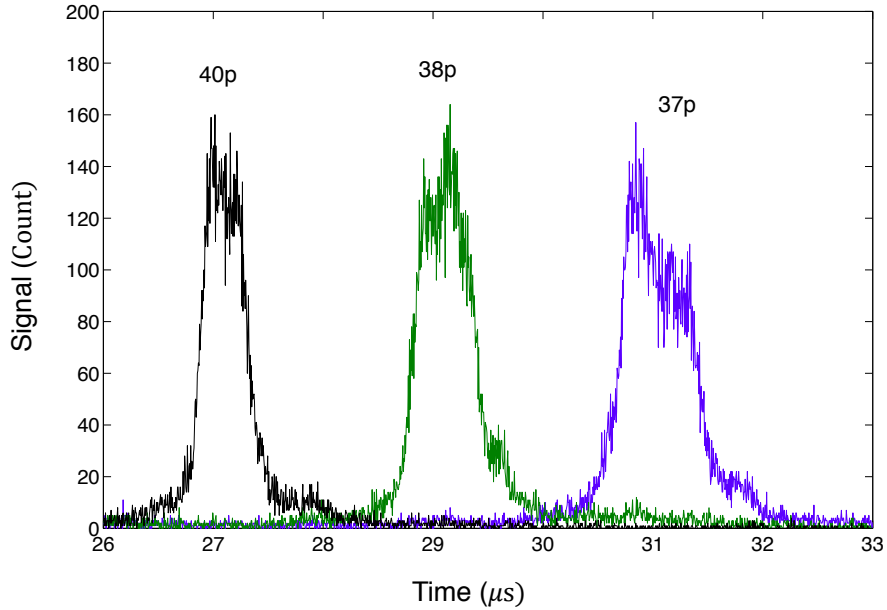

Figure: Time-resolved signals of lower Rydberg states detected by the field ionization method with plate separation of $\sim$ 1.35 cm.

Detection of Rydberg atoms with field ionization

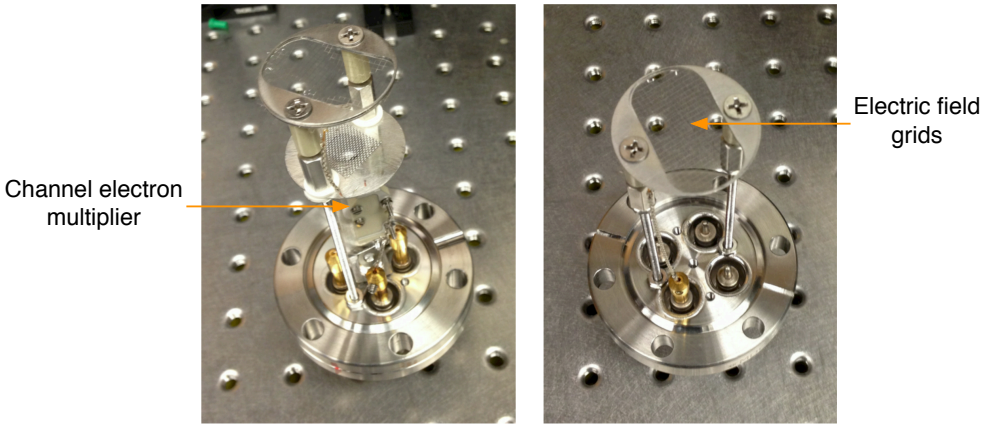

Figure: Ion detection system before installation in the vacuum chamber. (a) The assembly for the channel electron multiplier. (b) The assembly of the plate used for field ionization of Rydberg atoms.

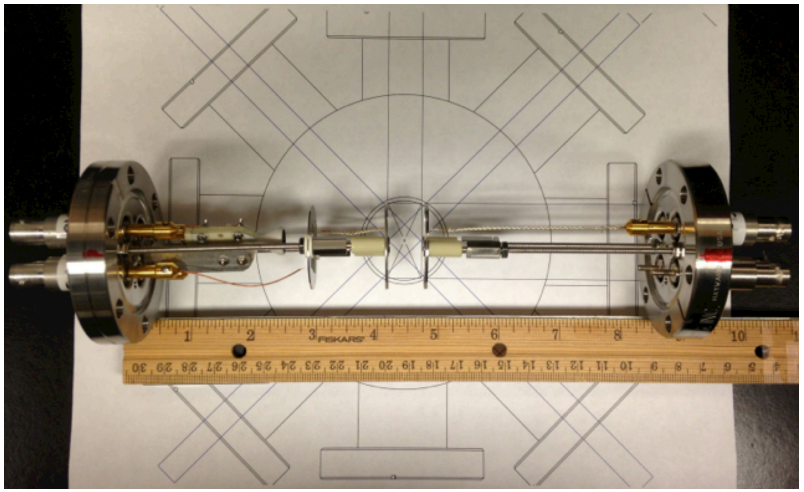

Figure: Geometry of the ion detection system. The magneto-optical trap beams enter the central region of the vacuum chamber through the slots in the steel plates covered with transparent nickel mesh.

Detection of Rydberg atoms with field ionization

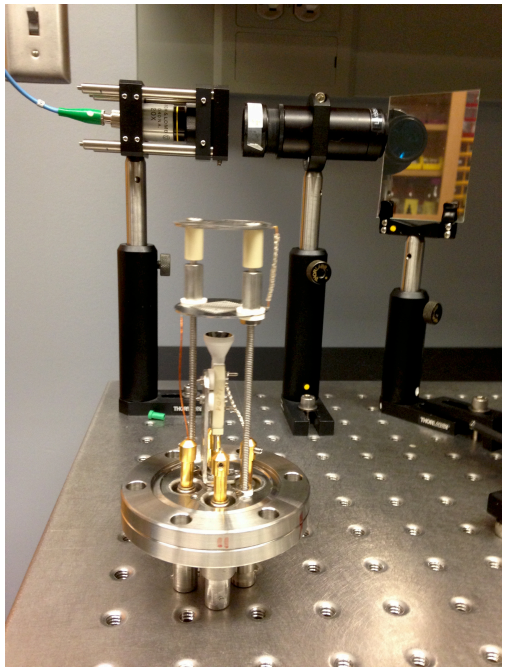

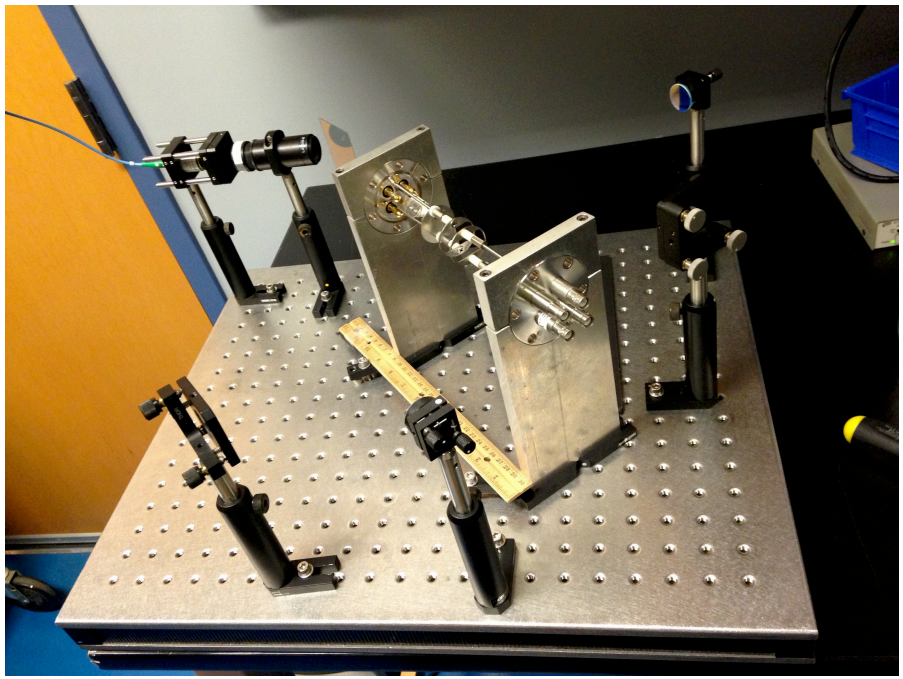

Test assembly of the ion detection system before installing into the vacuum chamber.

Detection of Rydberg atoms with field ionization

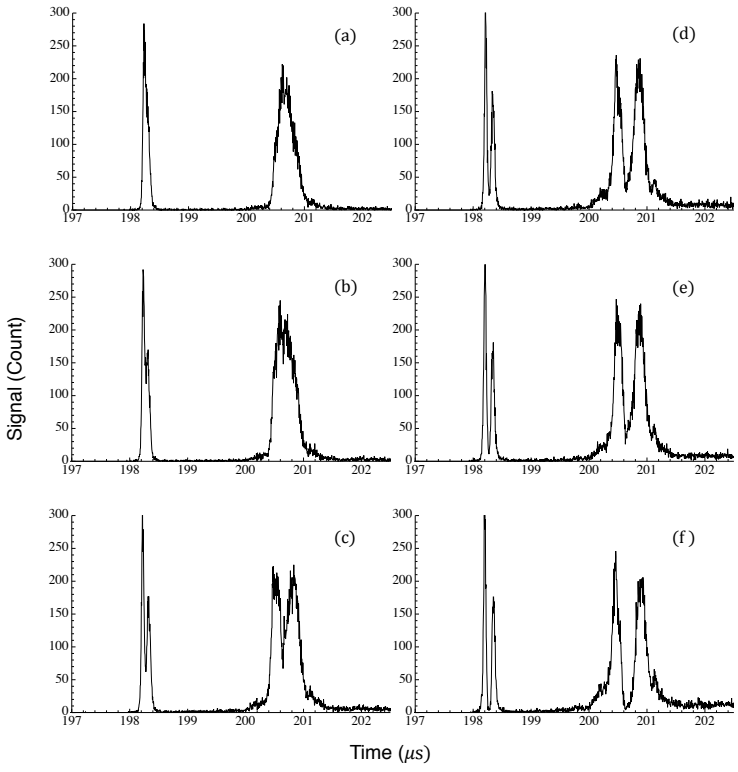

Figure: Signals of the $45d$ state at various energies of the excitation pulsed laser beam. The energies from (a) to (f) are $\sim$ 20, 30, 40, 60, 75, and 90 μJ/pulse respectively.

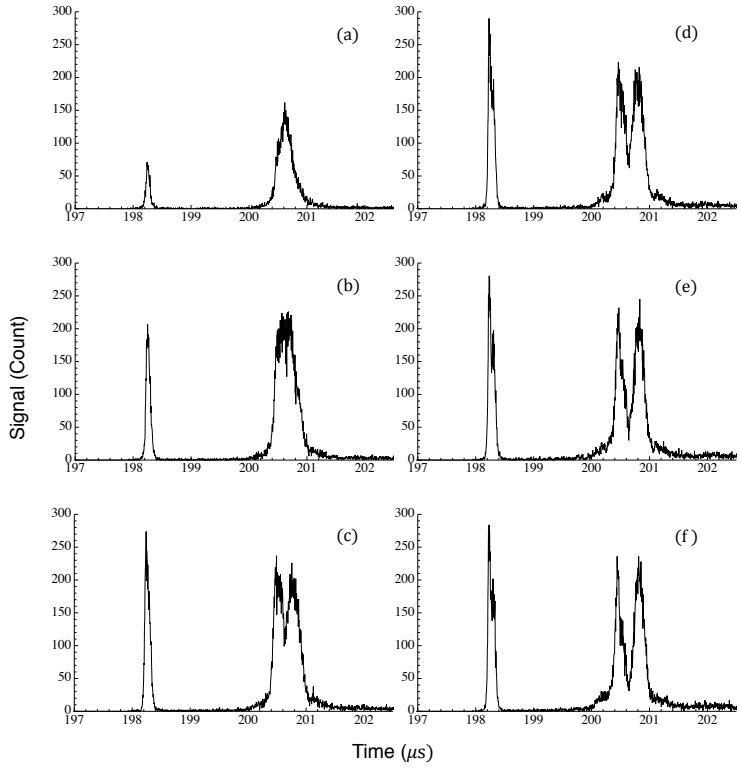

Figure: Signals of the $45d$ state at various densities of the magneto-optical trap. The trap density is varied with the intensity of the trap laser beams. The intensities from (a) to (f) are $\sim 9, 15, 20, 26, 30, 35$, and 38 mW/cm^2 respectively.

Experimental timing sequence

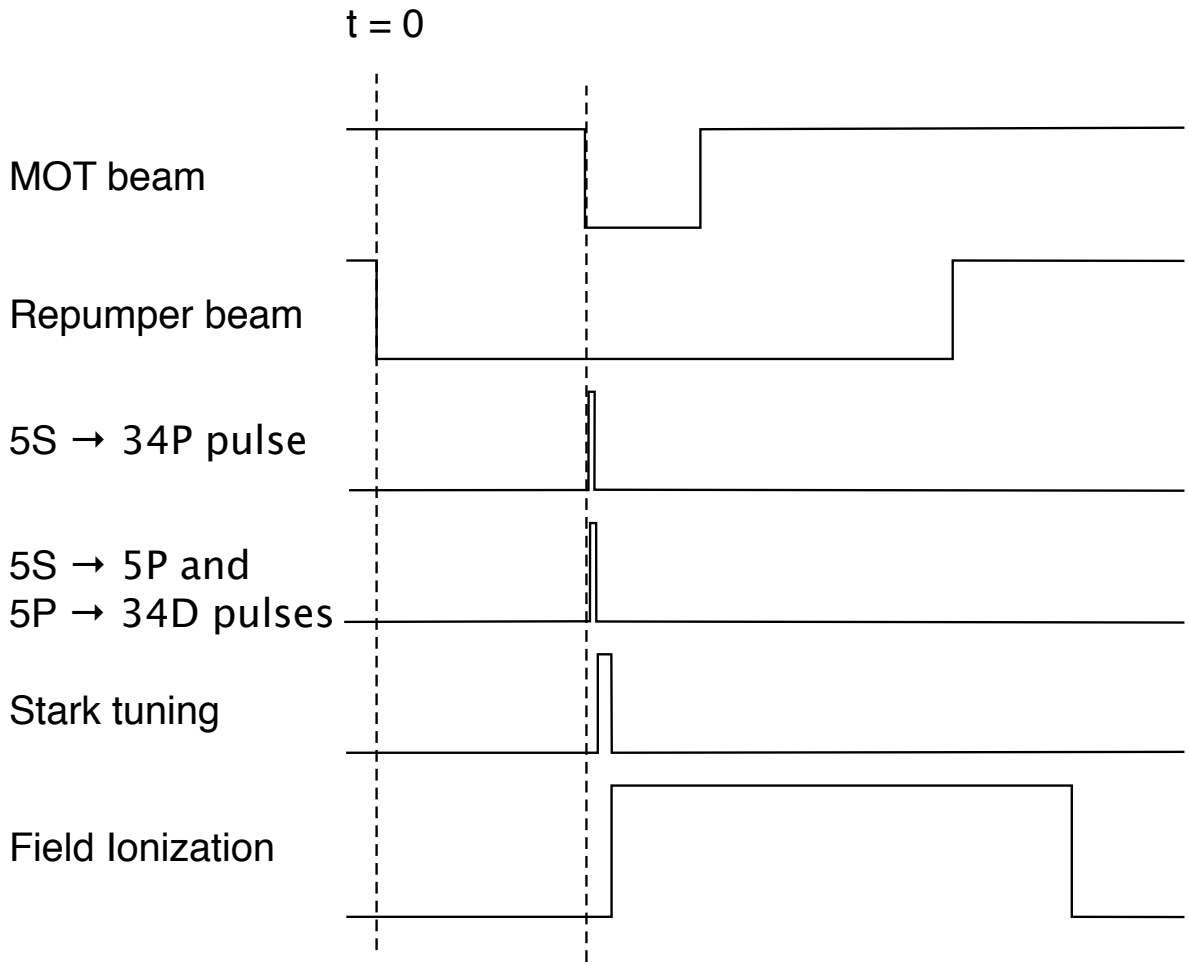

Figure: Experimental timing diagram.

Observation of Stark-tuned Förster resonances

$34p + 34p \rightarrow 34s + 35s$

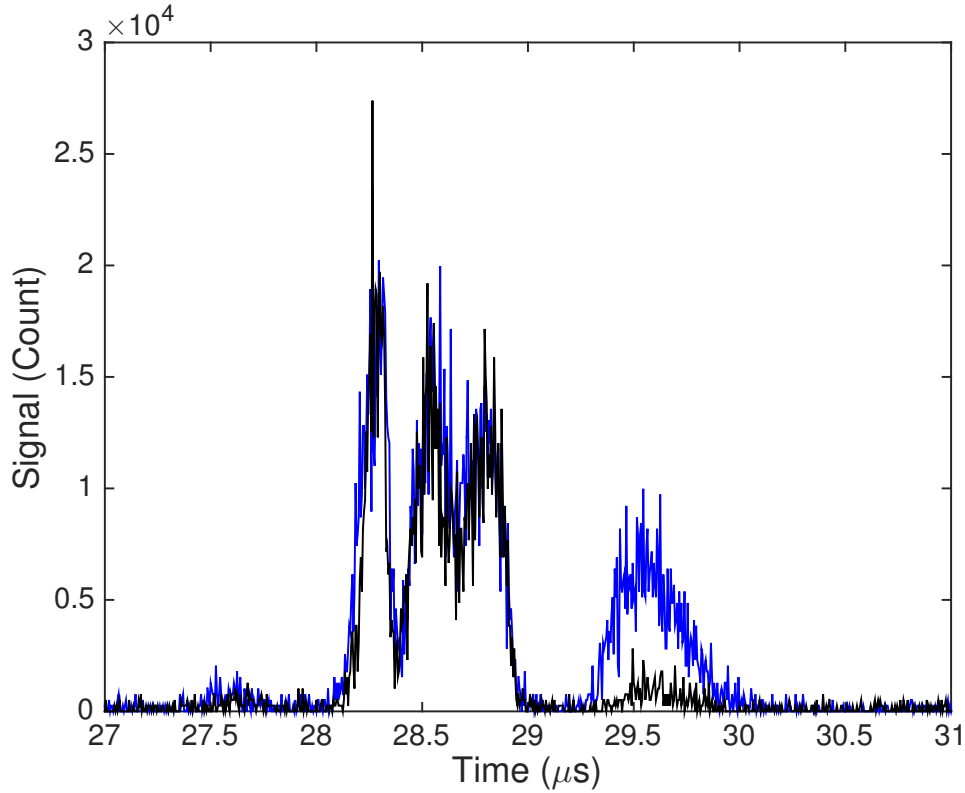

Figure: Time-resolved signals of Rydberg states for the process $34p_{3/2} + 34p_{3/2} \rightarrow 34s_{1/2} + 35s_{1/2}$. The signal in blue is for the resonant electric field, and the signal in black is for the non-resonant electric field.

Observation of Stark-tuned Förster resonances

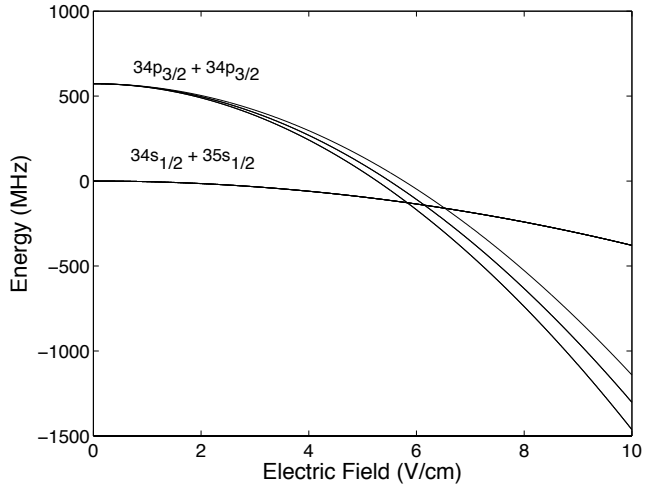

Figure: Stark structures of the pair states.

Table: Calculated electric fields for Förster resonances.

Process	Electric field (V/cm)
$34p_{3/2,\|1/2\|} + 34p_{3/2,\|1/2\|} \rightarrow 34s_{1/2} + 35s_{1/2}$	5.83
$34p_{3/2,\|3/2\|} + 34p_{3/2,\|1/2\|} \rightarrow 34s_{1/2} + 35s_{1/2}$	6.16
$34p_{3/2,\|3/2\|} + 34p_{3/2,\|3/2\|} \rightarrow 34s_{1/2} + 35s_{1/2}$	6.53

Observation of Stark-tuned Förster resonances

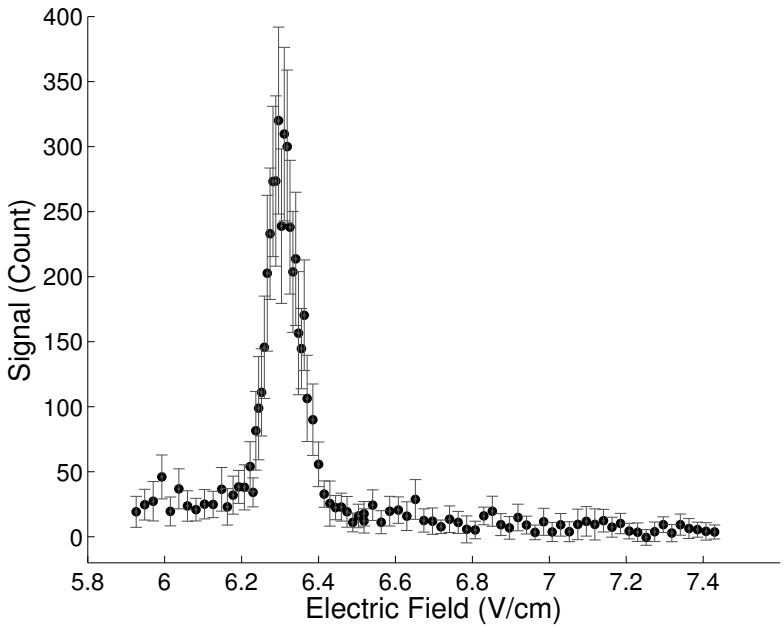

Figure: Förster resonance for the process $34p_{3/2,|1/2|} + 34p_{3/2,|1/2|} \rightarrow 34s_{1/2} + 35s_{1/2}$. The polarization of the excitation laser beam is set to be in the z direction.

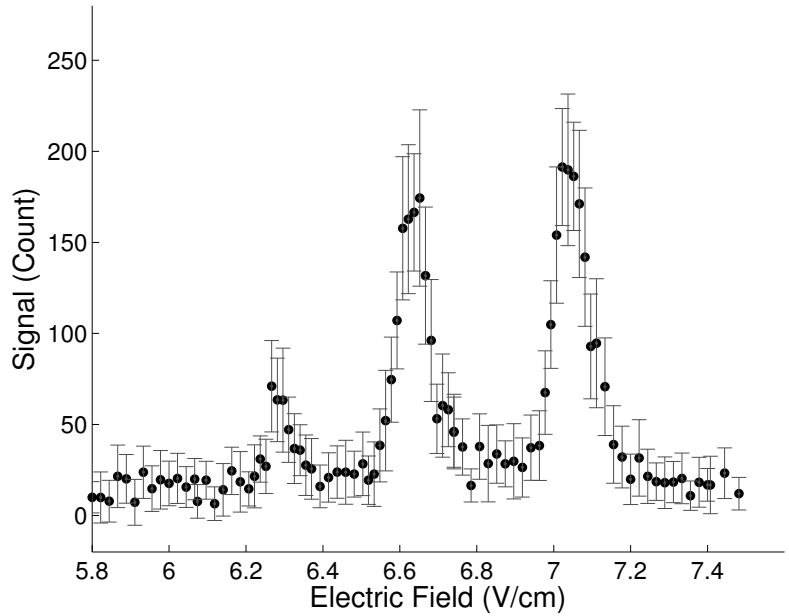

Figure: Förster resonances. The polarization of the excitation laser beam is set to be in the x direction.

Resonances observed at 6.3 V/cm, 6.6 V/cm, and 7.1 V/cm.

Catalysis of Stark-tuned interactions

- $34p + 34p \rightarrow 34s + 35s$
  Resonant at certain electric fields.

- $34p + 34s \rightarrow 34s + 34p$, and

  $34p + 35s \rightarrow 35s + 34p$

  Resonant for all electric fields.

- Introduce $34d$ state atoms into the interaction.
  An additional always resonant interaction channel

  $34p + 34d \rightarrow 34d + 34p$

Observation of catalysis of Stark-tuned interactions

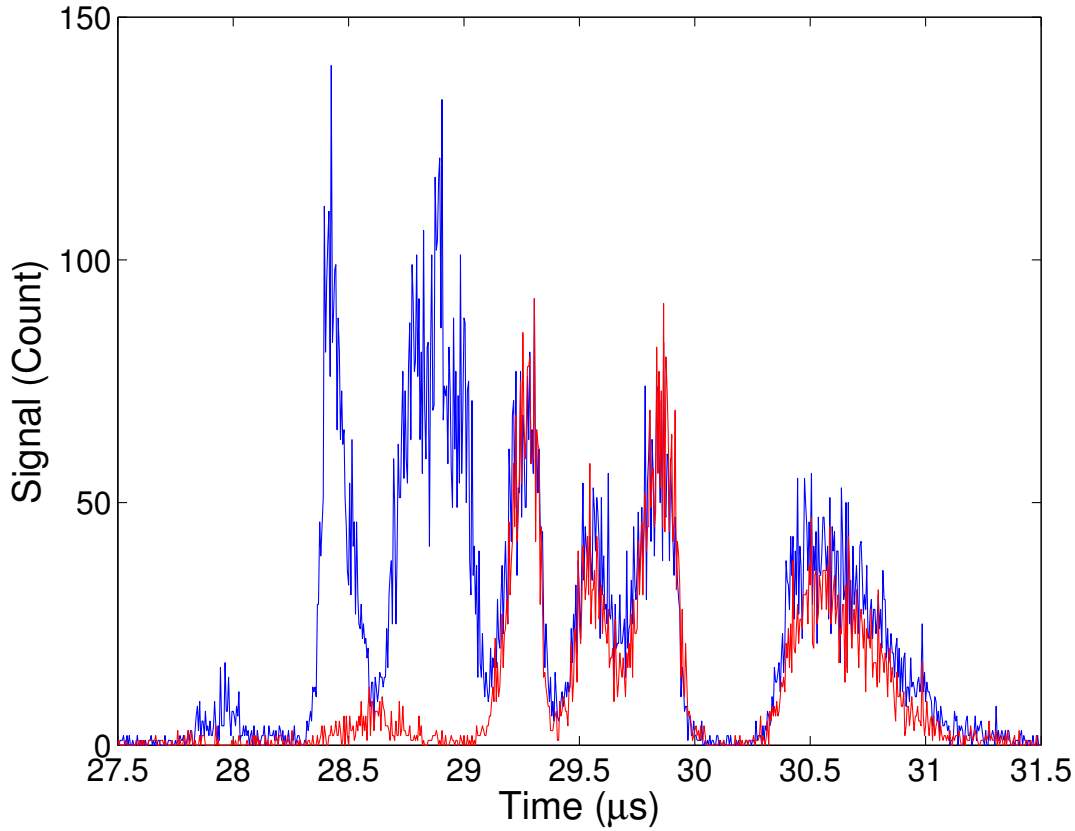

Figure: The signals of Rydberg states $34d, 34p$ and $34s$ for the interaction time of 7μs in the resonant electric field for $34p_{3/2,|m_j|=1/2} + 34p_{3/2,|m_j|=1/2} \rightarrow 34s_{1/2} + 35s_{1/2}$. The signal in red is for the interaction without $34d$ state Rydberg atoms, and the signal in blue is for the interaction with $34d$ state Rydberg atoms included.

Observation of catalysis of Stark-tuned interactions

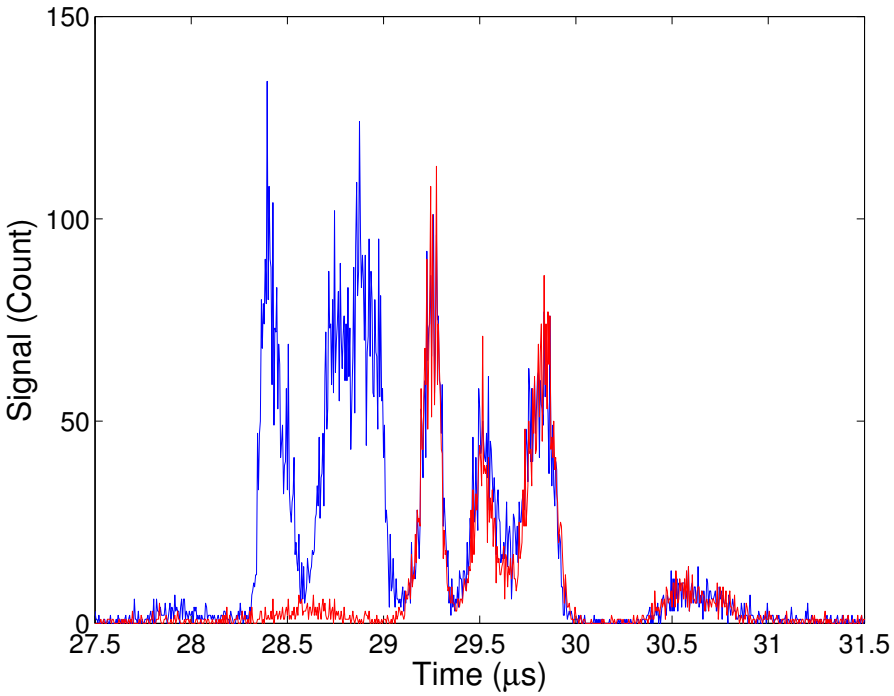

Figure: The signals of Rydberg states $34d$ and $34p$ for the interaction time of 7μs in a non-resonant electric field.

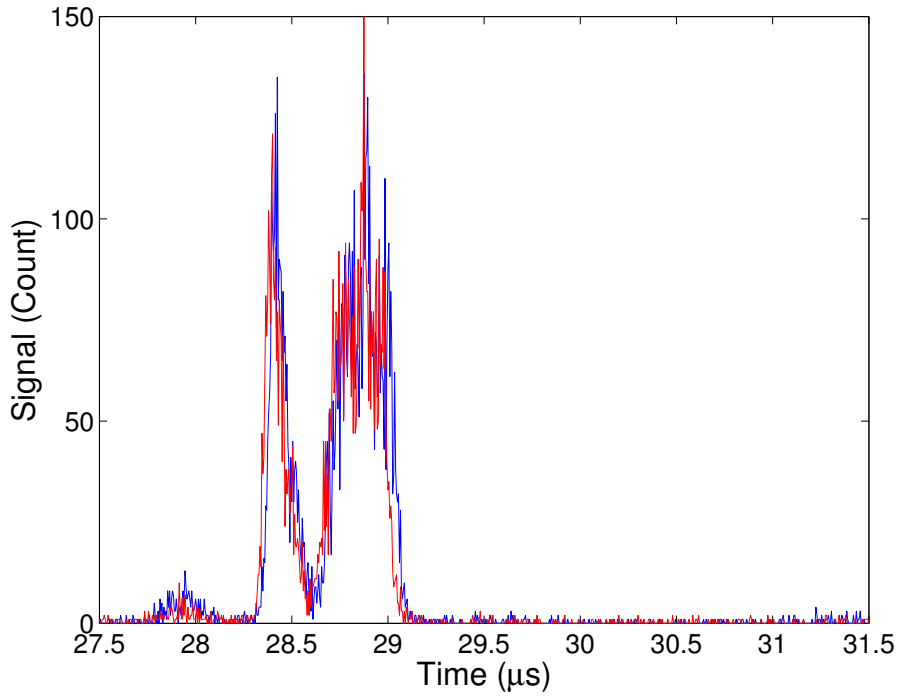

Figure: The signals for $34d$ state only for the interaction time of 7μs in the resonant (blue) and non-resonant electric field (red).

Interaction time dependence

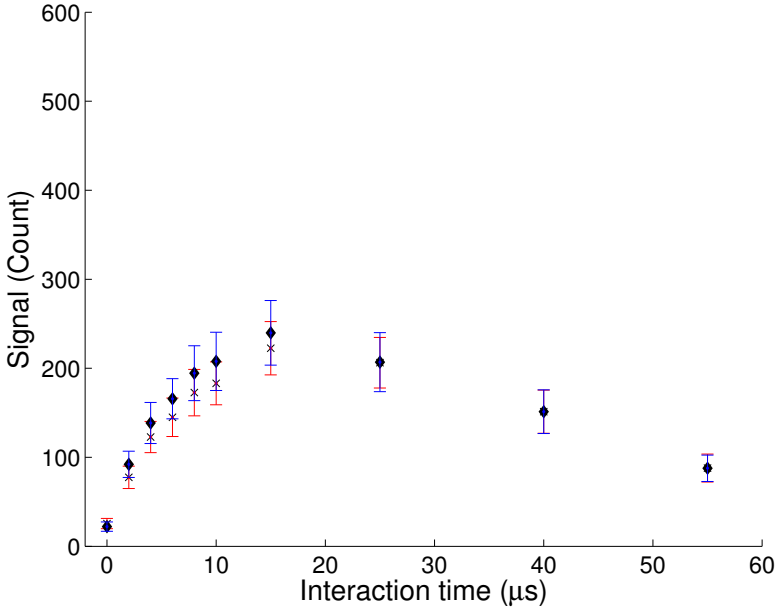

Figure: Interaction time dependence of the $34s$ state population for $34p_{3/2,|m_j|=1/2} + 34p_{3/2,|m_j|=1/2} \rightarrow 34s_{1/2} + 35s_{1/2}$. The data in the symbol $\times$ is for the process without the $34d$ state atoms included in the interaction, and that in symbol $\blacklozenge$ is for the process with the $34d$ atoms in the interaction.

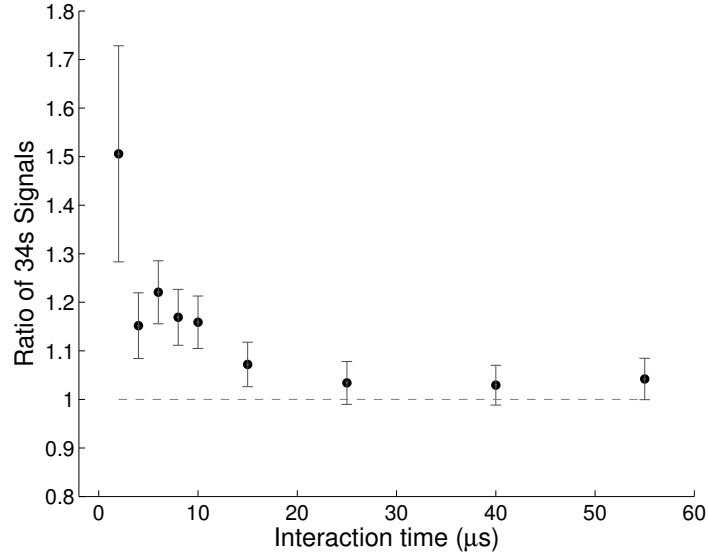

Figure: Ratio of the $34s$ state population vs. interaction time with and without $34d$ included in the interaction for the resonant energy transfer process $34p_{3/2,|m_j|=1/2} + 34p_{3/2,|m_j|=1/2} \rightarrow 34s_{1/2} + 35s_{1/2}$.

Interaction time dependence

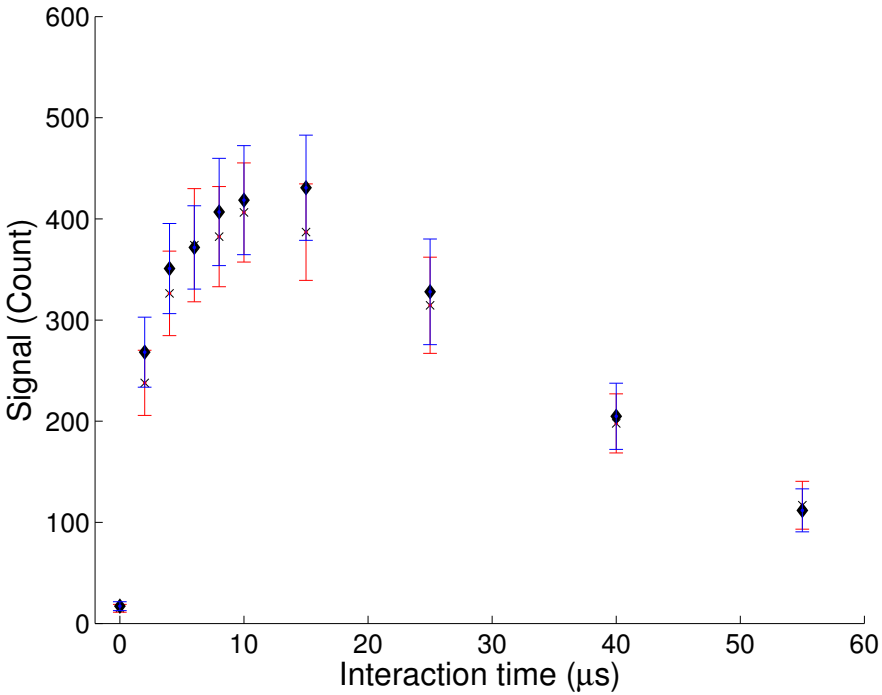

Figure: Interaction time dependence of the $34s$ state population for $34p_{3/2,|m_j|=3/2} + 34p_{3/2,|m_j|=1/2} \rightarrow 34s_{1/2} + 35s_{1/2}$.

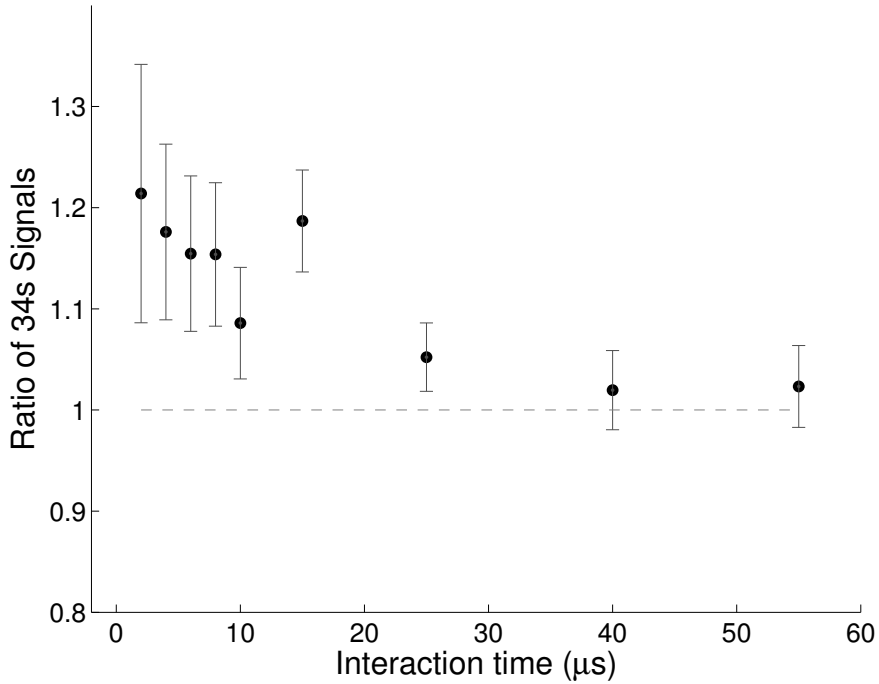

Figure: Ratio of the $34s$ state population vs. interaction time with and without $34d$ included in the interaction for the resonant energy transfer process.

Interaction time dependence

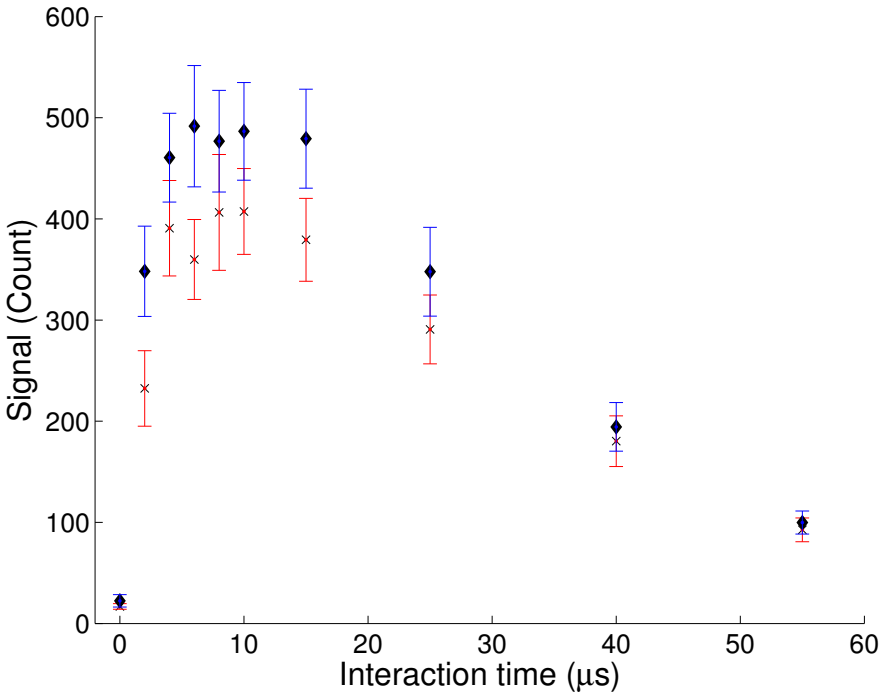

Figure: Interaction time dependence of the $34s$ state population for $34p_{3/2,|m_j|=3/2} + 34p_{3/2,|m_j|=3/2} \rightarrow 34s_{1/2} + 35s_{1/2}$.

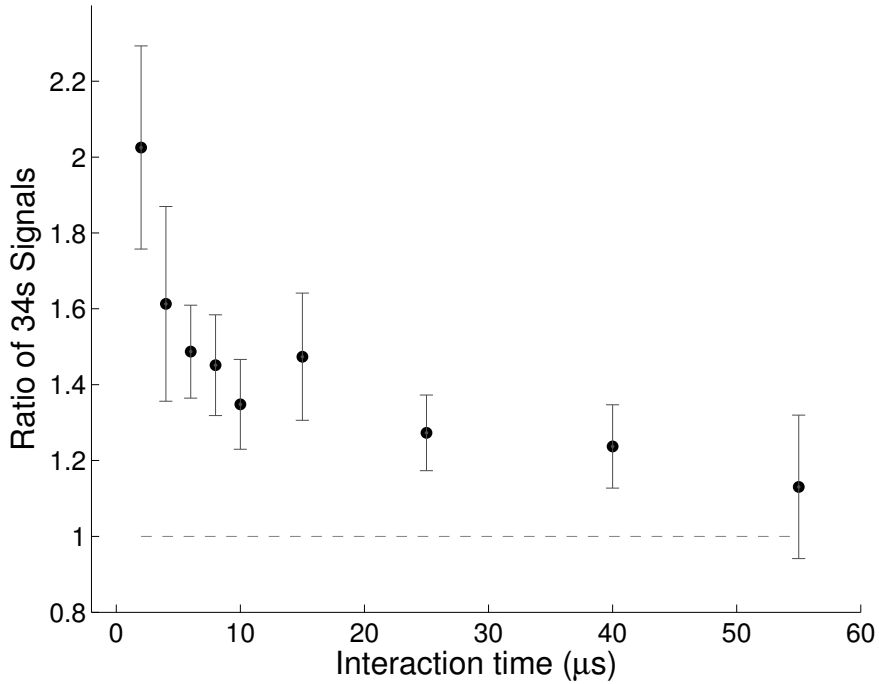

Figure: Ratio of the $34s$ state population vs. interaction time with and without $34d$ included in the interaction for the resonant energy transfer process.

Models for time dependence of the interaction

$34p + 34p \rightarrow 34s + 35s$

Simple models based on models developed by Westermann et al. [8]
Frozen Rydberg gas approximation [1, 5]

Two-atom model
The basis states for the two-atom model are

$$|pp\rangle,$$
$$|ss'\rangle, \text{and}$$
$$|s's\rangle.$$

These states are coupled by the dipole-dipole interaction, V_{dd}. For example,

$$\langle pp|V_{dd}|ss'\rangle = \frac{\mu_1\mu_2}{R^3},$$

where $\mu_1 = \langle p|r|s\rangle$ and $\mu_2 = \langle p|r|s'\rangle$ are the dipole matrix elements, and R is the distance between the two atoms.

Models for time dependence of the interaction

To find the time evolution of the fraction of s' atoms we numerically solve the time dependent Schrödinger equation.

$$i\hbar \frac{dc_j(t)}{dt} = \sum_k c_k(t) H'_{jk},$$

where $c_j(t)$ and $c_k(t)$ are the time dependent probability amplitudes for the basis states $|\phi_j\rangle$ and $|\phi_k\rangle$ respectively, and $H'_{jk} = \langle \phi_j | V_{dd} | \phi_k \rangle$.

number of atoms	2	3	4	6	8	10
number of states	3	7	19	141	1107	8953

Interaction time dependence

6.9×10^6 atoms/cm^3 $\quad$ 2.5×10^7 atoms/cm^3 $\quad$ 2.8×10^7 atoms/cm^3

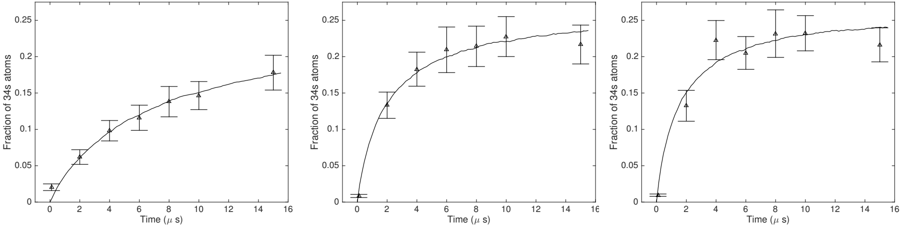

The time evolution of the fraction of 34s atoms for each resonant energy transfer process. The experimental data is scaled to fit to simulation with the six-atom model.

Interaction time dependence

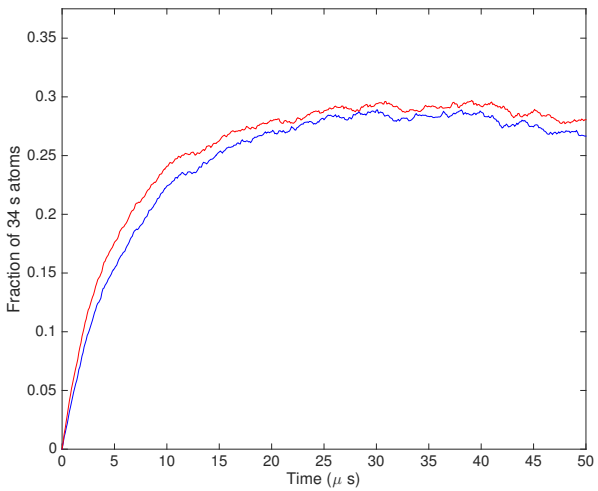

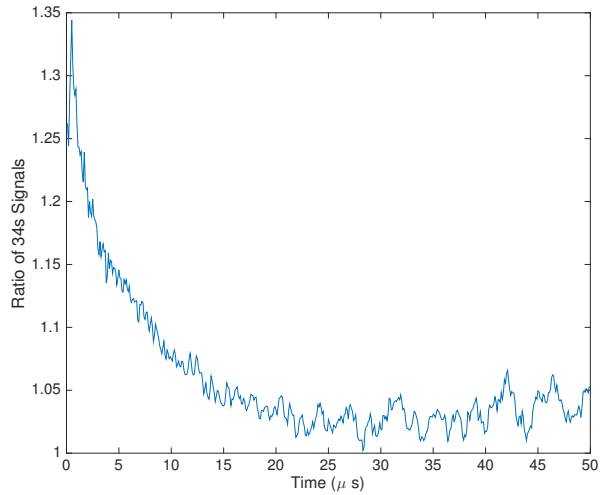

Preliminary simulation results with a simple three-atom model with d state atom placed midway between p state atoms. The matrix element $\langle p|r|d\rangle$ is set at an arbitrary value for this simulation.

Interaction time dependence

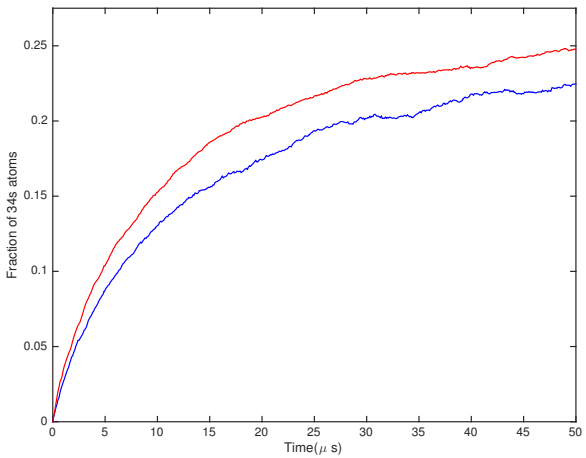

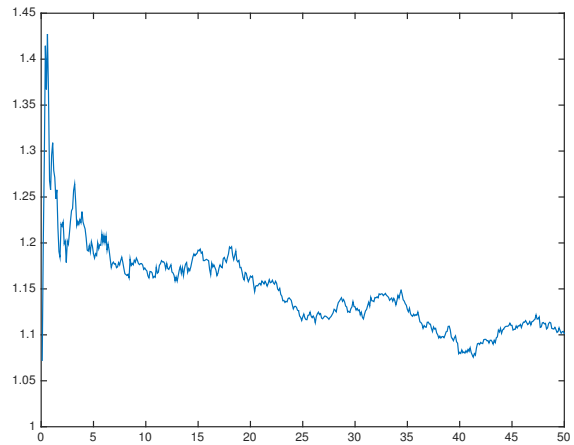

Preliminary simulation results with a six-atom model with four d state atoms placed midway between two p state atoms. The matrix element $\langle p|r|d\rangle$ is set at an arbitrary value for this simulation.

Summary and outlook

Summary

- Interactions between ultracold Rydberg atoms
- Stark-tuned Förster resonances
- Experimental setup
- Time dependence of resonant energy transfer process and observation of a catalysis effect in the resonant energy transfer between ^{85}Rb Rydberg atoms

Outlook

- Develop models with more atoms to simulate the observed catalysis effect.
- Investigation of the coupling strength dependence of the catalysis effect with different states other than $34d$ state.

Thank you!

Interaction of Rydberg atoms

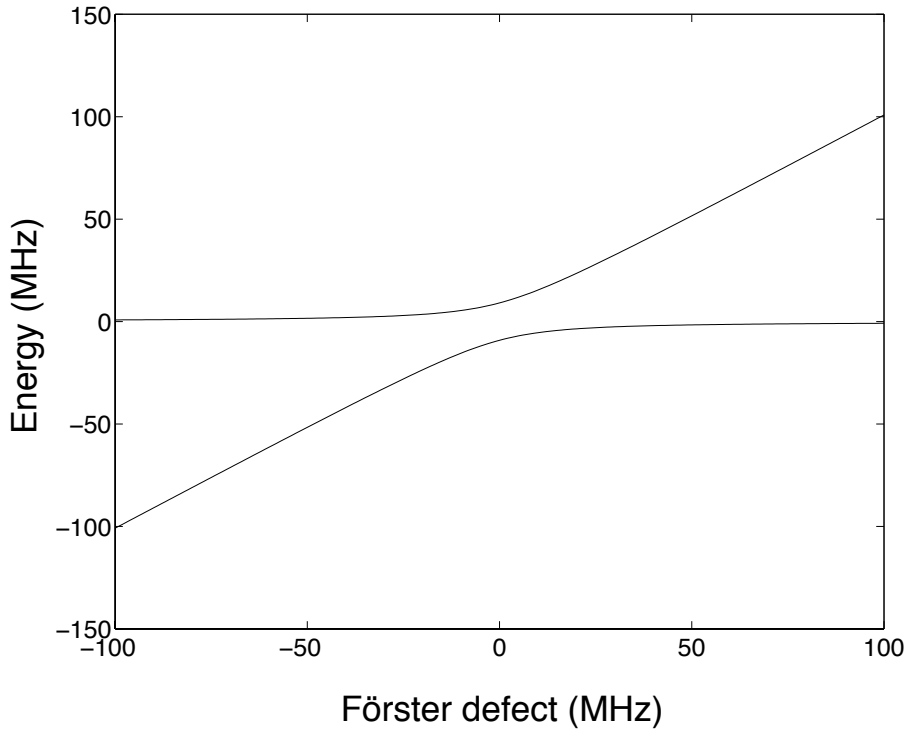

Figure: The energy shifts for the resonant dipole interaction of $34p_{3/2} + 34p_{3/2} \rightarrow 34s_{1/2} + 35s_{1/2}$ vs. Förster defect. The resonant dipole interaction energy $\mu_1\mu_2/r^3$ is $\sim$9.2 MHz for the distance between atoms of 5 μm.

Stark structure of Rydberg atoms

Stark Effect - atom in an external electric field

$$H = H_{atom} + Ez$$

The second-order energy shift

$$\Delta E_{Stark} = \sum_{nlm \neq n'l'm'} \frac{|\langle nlm|Ez|n'l'm'\rangle|^2}{E_{n'l'm'} - E_{nlm}}$$

When the Stark energy shift is comparable to the energy difference to the next dipole coupled state, the diagonalization of the Hamiltonian of the atom in the external electric field is necessary.

Rydberg atoms

Rydberg atoms are highly excited atoms.
In 1888 Rydberg discovered that the wavenumbers for different series of the observed lines of alkali atoms can be expressed as [2]

$$\nu_l = \nu_{\infty l} - \frac{R_y}{n^{*2}}, \tag{1}$$

where $n^* = (n - \delta_{nlj})$, the constant δ_{nlj} being quantum defect of the series l, $\nu_{\infty l}$ is the series limit, and $R_y = 109721.6$ cm $^{-1}$ is the Rydberg constant.

The energy of a Rydberg state is given by

$$W = -\frac{k^2 Z^2 e^4 m_e}{2n^{*2}\hbar^2}. \tag{2}$$

Rydberg constant is

$$R_y = \frac{k^2 Z^2 e^4 m_e}{2\hbar^2}, \tag{3}$$

where $k = 1/4\pi\epsilon_0$, Z is the atomic number, e is the charge of electron, m_e is the mass of electron, and $\hbar$ is the Planck constant.

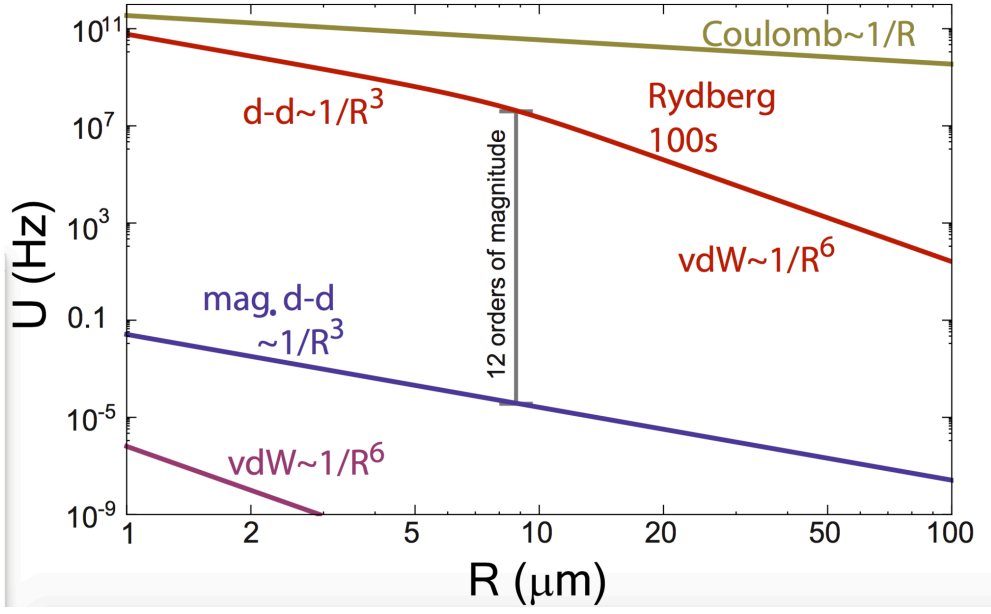

Figure: Two-body interaction strength for ground-state Rb atoms, Rb atoms excited to the 100s level, and ions. [6]

W. R. Anderson, J. R. Veale, and T. F. Gallagher.
Resonant dipole-dipole energy transfer in a nearly frozen rydberg gas.
Phys. Rev. Lett., 80:249–252, Jan 1998.

T. F. Gallagher.
Rydberg Atoms.
Cambridge University Press, 1994.

Michael G. Littman and Harold J. Metcalf.
Spectrally narrow pulsed dye laser without beam expander.
Appl. Opt., 17(14), Jul 1978.

Harold J. Metcalf and Peter van der Straten.
Laser Cooling and Trapping.
Springer, 1999.

I. Mourachko, D. Comparat, F. de Tomasi, A. Fioretti, P. Nosbaum, V. M. Akulin, and P. Pillet.
Many-body effects in a frozen rydberg gas.
Phys. Rev. Lett., 80:253–256, Jan 1998.

M. Saffman, T. G. Walker, and K. Mølmer.
Quantum information with rydberg atoms.

Rev. Mod. Phys., 82:2313–2363, Aug 2010.


Daniel A. Steck.
Rubidium 85 d line data.
http://steck.us/alkalidata/, Sep 2013.


S. Westermann, T. Amthor, A.L. de Oliveirab, J. Deiglmayr, M. Reetz-Lamour, and M. Weidemüller.
Dynamics of resonant energy transfer in a cold rydberg gas.
Eur. Phys. J. D, 40:37–43, June 2006.